STUDY OF THE POTENTIAL OF SUB-MILLIMETRE WAVE OBSERVATIONS FOR RAIN RETRIEVAL

E. Defer[(1)], C. Prigent[(1)], I. Meirold-Martner[(2)], J. R. Pardo[(3)], F. Aires[(4)], C. Walden[(5)], S. Crewell[(6)] , M. Mech[(6)], J.-P. Chaboureau[(7)], J.-P. Pinty[(7)], O.-Z. Zanifé[(8)]

[(1)] LERMA, CNRS-Observatoire de Paris, Paris, France
Email: eric.defer@obspm.fr, catherine.prigent@obspm.fr

[(2)]ACRI-ST, Sophia-Antipolis, France

[(3)] CAB, CSIC, Madrid, Spain

[(4)] LMD, CNRS-IPSL, Paris, France

[(5)] SSTD, RAL, Didcot, United Kingdom

[(6)] IMG, Köln University, Germany

[(7)] LA, CNRS-Université de Toulouse, Toulouse, France

[(8)] CLS, Ramonville Saint-Agne, Toulouse, France

ABSTRACT

Observations from geostationary satellites can provide the revisiting time necessary to monitor extreme weather events. However, from these orbits, passive microwave measurements at currently used frequencies require large antennas to achieve adequate spatial resolution. To overcome this problem, the use of millimetre (mm) and sub-millimetre (submm) wave observations is suggested. Radiometry at these wavelengths is predominantly sensitive to the cloud ice particles and rain detection/quantification is mainly derived from correlation with the ice particles above the rain. As application the Geostationary Observatory for Microwave Atmospheric Sounding (GOMAS) project submitted to the European Space Agency (ESA) proposes to operate multiple O_2 and H_2O channels on a GEO platform.

The main objective of the present study is to analyze the possible use of these high frequencies for rain detection and quantification and to assess how it complements the existing measurements. To analyze the relationship between rain and mm/submm wave observations, a dataset of simulated brightness temperatures (BTs) is created, using realistic atmospheric profiles derived from a cloud resolving model, and the statistical relationships between the BTs and the cloud and rain properties are examined. Several meteorological situations are modeled using Meso-NH, a 3D non-hydrostatic mesoscale model that simulates realistic meteorological flows. Meso-NH has an explicit cloud scheme that calculates the evolution of microphysical species (cloud droplets, raindrops, ice crystals, snowflakes and graupels). Radiative transfer calculations are performed with the Atmospheric Transmission at Microwaves model for different frequencies ranging from 23.8 to 875 GHz. It includes atmospheric gaseous absorption, scattering by hydrometeors, and surface emissivity estimates to calculate the expected microwave BTs. To evaluate the cloud model outputs and the radiative transfer computations, the simulations are also performed at operational sensor Advanced Microwave Sounding Unit (AMSU) and Special Sensor Microwave/Imager (SSM/I) frequencies for several atmospheric cases and are compared to AMSU and SSM/I satellite observations. For different specific frequency sets, including GOMAS, rain detection and rain rate retrieval based on supervised classifications and neural network schemes respectively have been developed and studied to determine their respective skills. The theoretical results indicate that errors below 50% are expected for rain rate above 1 mm/h for a mission such as GOMAS. The methodology has also been evaluated by comparing rain retrieval at close-to-mm AMSU-B observations and concurrent ground-based Chilbolton Advanced Meteorological Radar (CAMRa) rain measurements.

The potential of mm/submm wave observations for both precipitation detection and quantification has been demonstrated from theoretical calculations. This opens new perspectives to detect, quantify and track precipitation quasi-continuously on geostationary missions. The next step requires the development of airborne demonstrators, using mm/submm technology now available in European laboratories, to validate instrumental concepts and improve retrieval schemes.

1. METHODOLOGY

We detail here the results of the last stage of a three-step study. The first step of study deals with performing realistic cloud simulations with a cloud model [1]. The second step focuses on the computation of brightness temperatures (BTs) at different frequencies with the help of a radiative transfer (RT) model [2]. Finally we assess, relatively to the Eumetsat User position paper [3] (Table 1), the ability of different frequency sets to detect rain and quantify the rain rate as described in detail in [4] and [5].

Table 1. User requirement table related to liquid precipitation, based on the EUMETSAT position paper [3].

			Accuracy (r.m.s.)		
Parameter	Application	Unit	threshold	breakthrough	objective
Precipitation profile (liquid)	NWP global	%	100	50	20
	NWP regional	%	100	50	20
Precipitation rate at surface (liquid)	NWP global	%	100	50	20
	NWP regional	%	100	50	20
	Climate	mm/h	10	5	2
	Hydrology (>10mm/h)	%	20	10	5
	Hydrology (1-10mm/h)	%	40	20	10
	Hydrology (<1mm/h)	%	80	40	20
Precipitation detection (liquid)	NWP global	HR/FAR	50/50	95/10	99/2
	NWP regional	HR/FAR	50/50	95/10	99/2
	NWC	HR/FAR	50/50	70/40	85/20
Precipitation Type	NWP global	classes	3	4	6
	NWP regional, NWC	classes	3	4	6
	Climate	classes	3	4	6

1.1 The database of atmospheric profiles and the associated brightness temperatures

1.1.1 Simulation of realistic atmospheric scenario

Five mid-latitude European meteorological situations have been simulated that represent a large variety in rain rate distribution but also in terms of precipitation nature. The cloud-resolving model Meso-NH is used to provide a detailed description of the atmosphere including the hydrometeor distribution of five hydrometeor types (rain, cloud, ice, graupel, and snow). Reference [1] describe the setup of the cloud simulations as well as the different processes implemented in the cloud model, detail cloud and precipitation variability of the cloud simulations and show that the mid-latitude database is complementary to the Goddard PROFiling (GPROF) database [6]. The cloud simulations were performed with a two-way grid nesting technique with a 50-layer configuration and with a depth of the vertical grid ranging from 60 to 600 m. Each meteorological situation covers roughly a region of 1600 km x 1600 km and for each situation two time steps representative of the evolution of the situations are available.

1.1.2. Radiative transfer simulation

The cloud model simulations are used as entries to the RT model Atmospheric Transmission at Microwaves (ATM, [7]). The RT model includes an up-to-date gaseous absorption scheme validated up to frequencies of 1.6 THz [8]. The radiation scattering by oblate or prolate spheroids is calculated with T-matrix algorithms [9]. The emissivity of the wind-roughened ocean surface is calculated using [10]. The land surface emissivity is estimated from atlases derived from SSM/I observations [11], along with angular and frequency parameterization [12]. Multiple scattering calculations are based on the adding-doubling method and originate from [13]. Reference [2] study the sensitivity of the microwave simulations to the hydrometeor properties for the present database and discuss the importance of a correct representation of the snow particles (density, refractive index, shape) in mid-latitude clouds in a radiative point of view. The RT computation performed here uses the cloud content provided by the cloud model on a 10-km grid. It is assumed that the microphysics is spatially uniformly distributed over each grid point.

1.1.3. Evaluation of Meso-NH / ATM combination with satellite observations up to 190 GHz

Since the quality of statistical retrieval algorithms is directly related to the realism of the simulated database, it is crucial to evaluate the quality of the simulations. Given that the Meso-NH calculations correspond to real atmospheric situations, comparisons have been performed between Meso-NH/ATM simulations and satellite observations at

frequencies up to 190 GHz using Special Sensor Microwave/Imager (SSM/I, between 19 and 85 GHz) and Advanced Microwave Sounding Unit (AMSU, between 22 and 190 GHz) [2]. Such a comparison for a large range of frequencies is very challenging: each frequency is sensitive to a large set of atmospheric and surface parameters, imposing very strong constraints on the quality of both the Meso-NH simulations and the radiative transfer model. SSM/I frequencies are more sensitive to the lower part of the atmospheric column, including the surface contribution. The AMSU-B window channel at 150 GHz is particularly responsive to scattering by frozen particles. In addition, IR responses have been simulated with RTTOV [14] and compared to the METEOSAT images [1]. The comparisons show an overall good agreement between the simulations and the observations but first revealed an underestimation of the scattering by frozen particles at microwaves above 80 GHz (especially at 150 GHz). A careful analysis made it possible to overcome the discrepancy, by defining more accurately the scattering properties of snow in the cloud [2].

1.1.4. Frequency selection

Satellite projects in the millimetre and sub-millimetre wavelengths such as Geostationary Observatory for Microwave Atmospheric Sounding (GOMAS, [15]) on a geostationary orbit or Cloud Ice Water Sub-millimeter Imaging Radiometer (CIWSIR, [16]) on a polar orbit propose frequency channels that have similarities but are not identical, mainly because their objectives are not exactly the same: GOMAS being originally focused on water vapor and temperature profiling and more recently on precipitation, and CIWSIR on cirrus characterization. The relationships between the frequency responses and the hydrometeor profiles are complex, non-linear, and regime dependent. In the present study simulations are performed at a large number of frequencies, in window channels as well as in H_2O and O_2 lines (Table 2), covering the frequency range from 20 GHz to 900 GHz. A total of 37 frequencies have been simulated for all the profiles in the database, including the AMSU, GOMAS-like and CIWSIR-like frequencies and the 11-µm thermal IR channel (Table 2). Fig. 1 shows BT maps computed at 150, 301 and 462 GHz and 11 µm at nadir for one of the simulated atmospheric scenario. Fig. 1 also suggests that simultaneous measurements at multiple frequencies should be used to retrieve the atmospheric properties such as rain rate or vertically integrated content as we detail later. In the next sections various channel combinations are tested and compared for their potential to detect rain and to quantify the rain rate. The left panel in Fig. 2 lists the frequency sets investigated in this study. Nineteen different frequency combinations have been considered. F07 is of special importance in this study as it is close to the frequencies suggested for the geostationary project GOMAS. F09 is close to the channel selection for CIWSIR mission.

Table 2. List of the simulated frequencies and associated noise level.

Frequencies (GHz) or wavelengths (µm) [*noise (in K)*]	Characteristics
23.8 [*0.2*], 31.4 [*0.27*]	Low freq. windows
50.3 [*0.22*], 52.8 [*0.15*], 53.596+/-0.115 [*0.15*], 54.40 [*0.13*], 54.94 [*0.14*], 55.50 [*0.14*]	O_2 line 50GHz
89.0 [*0.37*], 150.0 [*0.84*]	Medium freq. windows
183.31 +/- 1 [*1.06*], 3 [*0.7*], 7 [*0.6*]	H_2O line 183GHz
220.5 [*1.0*], 301.0 [*1.0*], 462.5 *[1.0*], 684.0 *[1.0*], 875.0 [*1.0*]	High freq. windows
118.75 +/- 0.2 [*0.5*], 0.4 [*0.5*], 0.7 [*0.5*], 1.1 [*0.4*], 1.5 [*0.4*], 2 [*0.3*], 3 [*0.2*]	O_2 line 118GHz
325.15 +/- 0.5 [*1.0*], 2 [*1.0*], 7 [*0.9*], 25 [*0.9*]	H_2O line 325GHz
380.19 +/- 0.5 [*0.5*]	H_2O line 380GHz
424.76 +/- 0.3 [*0.5*], 0.6 [*0.5*], 1 [*0.5*], 1.5 [*0.4*], 2 [*0.4*], 4 [*1*]	O_2 line 424GHz
11	Thermal IR

1.1.5 The resulting database

Simulations for each frequency are performed for different incidence angles (0, 9, 19, 30, 40, 52°). The two orthogonal linear polarizations are calculated separately and are combined as in the AMSU cross-track scanner. From a geostationary orbit, the polarization combination will also depend upon the scanning angle and the areas in satellite coverage. In this study, polarization emanates essentially from the surface as the hydrometeors are assumed to be spherical. The initial atmospheric profile database consists of a pixel population of 48% over land, 40% over ocean and 12% over the coasts. Note that in this work, coastal pixels are ignored. The entire database consists of 10 situations (2 outputs from the simulation of 5 meteorological situations) with 157 (6 parameters (rain, cloud, ice, graupel, snow and water vapor) x 25 layers + 6 integrated quantities (rain, cloud, ice, graupel, snow and water vapor) + rain rate) cloud and rain parameters and 217 (6 angles x 36 microwave channels + 1 IR channel) brightness temperatures for each profile.

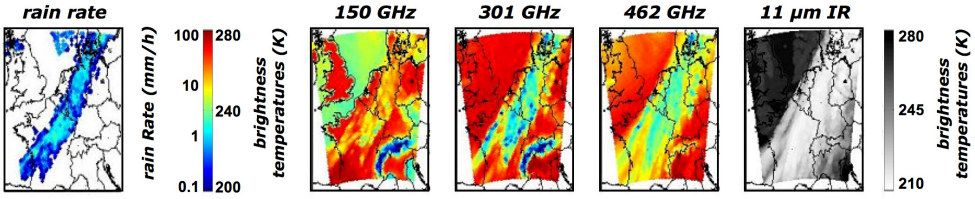

Fig. 1. Example of cloud/radiative simulations with rain rate as provided from the cloud model (left panel), and brightness temperatures computed from the atmospheric profiles at 4 different frequencies at nadir.

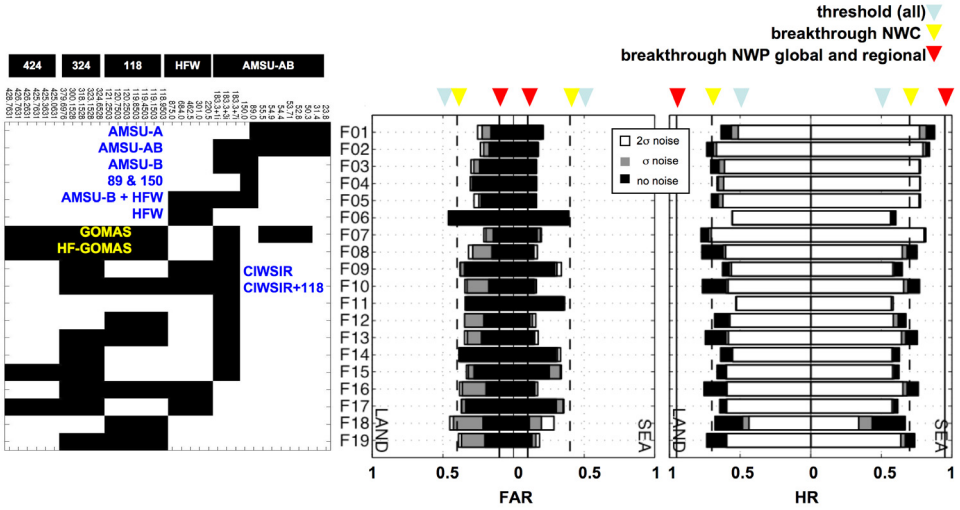

Fig. 2. Frequency combination (left panel) and associated false alarm rate (FAR) and hit rate (HR) for different noise levels for an incidence angle of 19° over sea and land separately.

1.2 Classification and retrieval methods

Situations over land and ocean are treated separately: the surface contributions to the brightness temperatures in the window channels below 150 GHz can be significant and the development of algorithms dedicated to each surface type usually improves the retrieval accuracy. For frequency sets limited to the mm/submm range, the sensitivity to the surface is reduced and the same algorithms could be used, but with restrictions for very dry atmosphere and/or regions with high elevations. The full scheme (classification + retrieval) is derived for each frequency set (listed in Figure 2), each incidence angle, and each surface type, and the performances are compared, for both rain detection and hydrometeor quantification. For each of the five meteorological situations considered in this study, two model outputs are available [1]: the first one is used for the training of the algorithms and the second one is used for testing the algorithms.

1.2.1 Rain classification

The development of a precipitation flag for a given observation is often the first step to quantify the rain from passive space borne observations. Instead of applying thresholds on selected channels, we apply a supervised classification method, based on the dataset of simulated brightness temperatures and atmospheric profiles used in this work. It allows for the combination of all investigated channels at once to benefit from their synergy. In addition, classifications are not limited to the binary precipitation/non-precipitation flag: distinction between different precipitation regimes can be derived in order to develop a regime-dependent retrieval scheme afterwards. Both two-class and multi-class classifications have been tested but the simple binary flag has finally been adopted (with a rain rate threshold at 0.1 mm/h). To evaluate the classification, the Hit Rate (HR = A/(A+C) (also called the Probability Of Detection, POD) and the False Alarm Ratio (FAR=B/(A+B)) are calculated, with A, B, C and D defined in the contingency table (Table 3).

Table 3. Definition of the contingency table.

	Rainy pixels	Non-rainy pixels
Classified as rainy pixels	A	B
Classified as non-rainy pixels	C	D

1.2.2 Rain retrieval algorithms

The database has been carefully analyzed to design an adequate pre-processing step. A Principal Component Analysis (PCA) of the atmospheric profiles is performed in order to compress the information, to reduce its dimension and to regularize the inversion process, which is important in particular for the retrieval of the atmospheric profiles. PCA is a powerful tool to extract uncorrelated pieces of information. Fifty PCA components are considered, representing 99% of the variance of the training database. The database of the selected PCA components and their associated brightness temperatures is then used to train two statistical algorithms: a multi-linear (ML) approach and a neural-network-based (NN) scheme. The NN scheme uses a Multi-Layer Perceptron trained by the back-propagation gradient descent algorithm and we present in the following the results obtained only with the NN scheme.

1.2 3. Evaluation of the retrieval schemes

The next step tests the algorithms to determine their performances. For a given set of brightness temperatures of the testing database, the corresponding algorithm is applied to estimate the hydrometeor quantities in the PCA basis, which are then projected into the initial atmospheric domain by applying the inverse PCA function. For physical parameters showing a large variability such as the rain rate, the sensitivity of the results to the error metric is large. In order to quantify the error between the true value x_i and the retrieved value r_i for each geophysical parameter, we compute the mean absolute relative error e_m as defined in (1). A second metric to measure the error is used for comparison with the thresholds discussed in the EUMETSAT position paper [3] (Table 1). The metric e_{rms} (2) corresponds to the r.m.s. of the relative error and includes both the random component and the bias error. Both errors are computed per rain rate range in order to assess changes in the retrieval performances as a function of the rain rate magnitude.

$$e_m = \frac{1}{N}\sum_{i=1}^{N}\frac{|r_i - x_i|}{x_i} \tag{1}$$

$$e_{rms} = \sqrt{\frac{1}{N}\sum_{i=1}^{N}\left(\frac{r_i - x_i}{x_i}\right)^2} \tag{2}$$

To summarize, for each frequency set, each observing incidence angle and each surface type (land and ocean), a rain detection scheme is developed, along with two statistical retrieval schemes (ML and NN algorithms) that estimate in addition to the rain rate the integrated contents of the five studied hydrometeor classes, as well as their vertical distribution. Given the large range of tested configurations (frequency combinations, angles, surface types, retrieval methods, retrieved variables) all the results are not systematically presented here. In the following we try to illustrate the major conclusions and to provide a synthetic analysis of these results, focusing on the rain paraameters.

1.2.4 Impact of the noise on the classification and the rain rate retrieval

Realistic instrumental noises have been added to the simulated BTs. The applied noises follow Gaussian laws with a standard deviation that depends upon the frequency (Table 1). Three noise configurations have been tested: one without any noise, one with the standard deviation set to the values of Table 1, and finally one with twice the noise from Table 1.

2. ASSESSMENT ON THE PERFORMANCES OF THE CLASSIFICATION

For the 19 different frequency sets, Figure 2 presents the scores of the classification for the same incidence angle (19°). HR and FAR breakthrough thresholds are indicated, for Numerical Weather Prediction (NWP) regional and global applications (95% and 10% respectively) and for nowcasting (70% and 40%). Results are plotted with overlaid bars in black for noise-free, in grey for 1σ noise and white for 2σ noise. As expected the classifications are less efficient when the noise increases. For nowcasting applications that are of primary concern from a geostationary orbit, FAR is usually well below the breakthrough threshold and HR is close to it for most combinations without noise added. In the presence of noise, only the F18 frequency combination (i.e. only 118 GHz channels) exhibits significant changes in both HR and FAR while for the other frequency sets the variations of HR and FAR are relatively limited. The classification at AMSU-A frequencies (F01) performs better over sea than over land according to its HR for the three noise configurations. This frequency combination has the highest HR over sea for the noise-free configuration and is slightly less efficient than the GOMAS configuration (F07) when the 2σ–noise configuration is applied: the low frequency

window channels provide the sensitivity to the rain emission over the oceanic cold background (related to the low ocean emissivity). Over land, the HR is higher when higher frequencies are used due to their sensitivity to scattering effects: scattering by the hydrometeors at high frequencies is observed over the high emissivity background. The frequency set corresponding to the high frequency window channels alone (F06) exhibits the lowest HR scores of all frequency ranges for all noise configurations as well as the highest FAR, for both sea and land pixels. When profiling capabilities are added (observations in O_2 and/or H_2O lines such as in the combination F09), the performances are improved. The frequency combination planned for a geostationary mission (F07) can provide a HR larger than 70% with a FAR of the order of 20%. This is within the breakthrough thresholds requested for nowcasting. Even if the lower frequency channels are suppressed for spatial resolution considerations (F08), HR remains close to the HR breakthrough threshold and FAR stays below the FAR breakthrough threshold. Suppressing the O_2 channels at 424 GHz does not significantly affect the results, as seen by the comparisons of the F08 and F13 sets, but suppressing the O_2 118 GHz channels does (compare F08 and F15). All the sets that do not have frequencies below 150 GHz (F06, F09, F11, F14, F15, F17) exhibit poor scores, even poorer at higher noise level, over land and ocean. It appears that the role of the sounding channel in O_2 lines (around 50 and/or 118 GHz) is significant, due to their potential to sound at different altitudes in the atmospheric column. However, it is also due to the fact that these frequencies are rather low compared to the other millimetre and sub-millimetre channels and penetrate deeper into the clouds. Note that the 118 GHz channels alone (F18) perform almost within the thresholds in the absence of noise but exhibits the worst performances when realistic noises are considered. Adding the 183 GHz set to the 118 GHz one (F12) does improve the results of the 118 GHz alone. The 118 O_2 and 325/380 H_2O combination (F19) yields acceptable performances, better than the 118 O_2/183 H_2O combination (F12). Adding the high window frequencies also helps the detection slightly (compare F19 and F16). The performances have been tested for the other incidence angles and the relative changes are insignificant.
In conclusion, the use of channels at rather low frequencies is necessary to provide good rain detection over ocean. Observations in high frequency window channels only are clearly not enough and sounding channels have to be added. For precipitation detection purposes, the 424 GHz observations are not necessary. A frequency set such as planned for GOMAS should provide precipitation detection within the threshold values, and close to them if the channels in the O_2 50 GHz lines are suppressed. Frequencies below 150 GHz (such as the 118 GHz sounding channels) will have to be added to an instrument like CIWSIR to detect precipitation with a suitable accuracy.

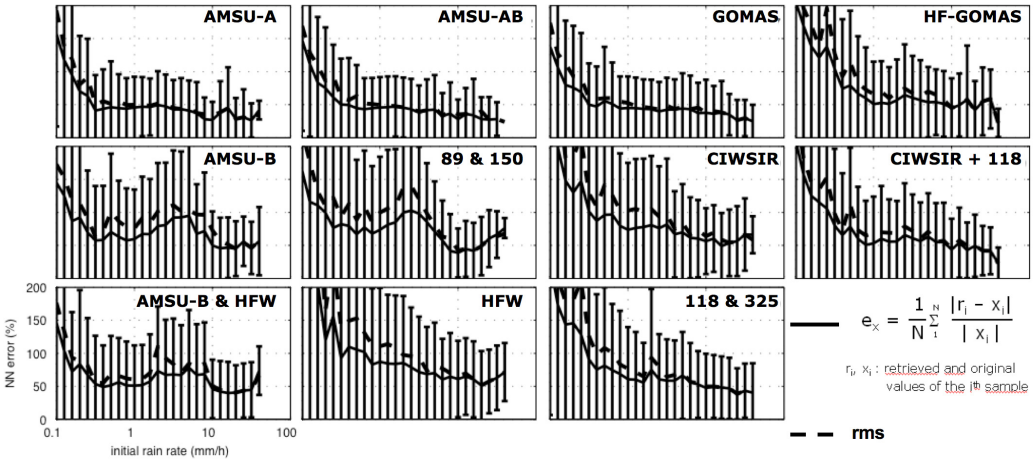

Fig. 3. Mean absolute relative error e_m (solid lines) +/- the standard deviations (vertical segment) and the r.m.s. errors e_{rms} (dashed line) computed per 0.1 bin for pixels over ocean at 19° incidence angle with the NN method for different frequency sets.

3. ASSESSMENT OF THE PERFORMANCES OF THE RETRIEVAL SCHEMES

For different frequency combinations Fig. 3 shows the errors e_{rms} and e_m along with the standard deviation around the error e_m (vertical segments), for the NN inversion over ocean at 19° incidence angle in a noise-free configuration. The errors usually decrease when RR increases. Note that e_{rms} and e_m can be significantly different, explaining in part the differences in the results obtained from one study to the other when the error definitions are not identical. At AMSU-A (F01), AMSU-AB (F03), or at frequencies selected for geostationary projects (F07, GOMAS in Fig. 3), the errors are within 50% for RR above 0.5 mm/h, i.e., are well within the threshold values of 100% requested for NWP application and below the breakthrough values of 50% (Table 1). However, all these measurement combinations are clearly not suitable for land surface hydrology applications given the accuracy specified in Table 1. Strong precipitation events

(RR > 10 mm/h) can be quantified with errors around 50% for all frequency configurations. A frequency combination similar to one of the CIWSIR mission (F09) does not provide the requested accuracy but the addition of the 118 GHz channel does improve the results. A simple instrument combining the 118 GHz O_2 and the 325/380 GHz H_2O (F19) sets yields performances close to the specifications for RR > 1 mm/h. Results for the F07 frequency set over ocean and land are comparable for all incidence angles (not shown). Adding the thermal infrared has almost no impact, except for the configurations that originally suffered from large errors (not shown). Introducing noise in the treatment induces small variations in the retrieval performances except for the F08 frequency set (HF-GOMAS) for low rain rates over ocean (not shown).
We also investigated the potential of mm/submm wave radiometry to retrieve vertically integrated hydrometeor content. Using a GOMAS-like frequency configuration, the average error for total-ice retrieval is below 40% and for most of the total-ice content range close or below 20% (not shown). This is within the threshold of 50% specified by the user requirements for this quantity and close to the 20% breakthrough value [3]. We also investigated the capability of a mission like GOMAS in retrieving hydrometeor profiles (not shown). Except for the very low rain content in the rain profil, the r.m.s. error is below the breakthrough threshold of 50% and for the sets that include low frequencies (F02 and F07) the r.m.s. error is larger than 100% only for the very low rain contents.

4. TESTING THE METHOD AT AMSU-B FREQUENCIES AGAINST RADAR OBSERVATIONS

In order to evaluate the rain rate inversion method, it is applied to close-to-millimetre wavelength observations (AMSU-B) and the results are compared to radar measurements. The two-step method is applied to the AMSU-B observations. First, the rain classification selects the rainy pixels then the inversion algorithm is applied to these pixels. The AMSU instrument is a cross-track scanner and for each beam position the algorithm corresponding to the incident angle is adopted. In the previous analysis, it was shown that the frequency combination corresponding to AMSU-B is not optimum and shows poorer performances than what is expected for the recommended channel sets. As a consequence, it is likely to underestimate the performances as compared to the recommended frequency combination. The AMSU-AB combination has not been tested due to the poorer spatial resolution at AMSU-A frequencies that would seriously hamper the comparison with radar scenes of limited extent.

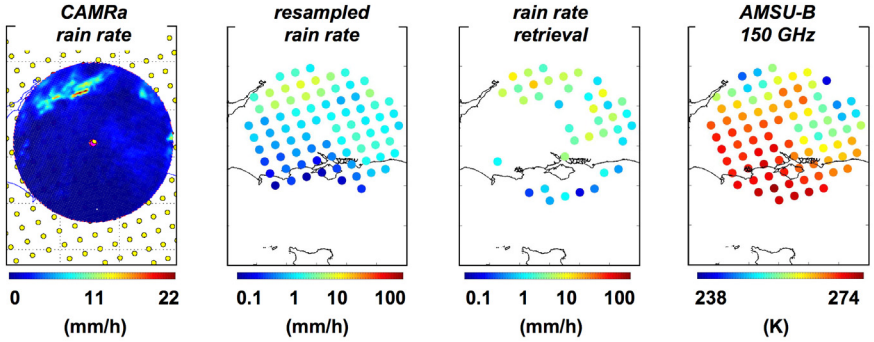

Fig. 4. Example of retrieval for one AMSU-B pass over the CAMRa domain. From left to right: map of high resolution CAMRa rain rate field, map of resampled CAMRa rain rate along AMSU-B beams, map of rain rate retrieved from the observations of the 5 AMSU-B channels and map of AMSU-B 150 GHz concurrent observations.

The Chilbolton Facility for Atmospheric and Radio Research established a set of ground validation test cases, by performing Chilbolton Advanced Meteorological Radar (CAMRa) radar scans during AMSU-B overpasses for both stratiform and convective cases. A total number of 1727 AMSU beams colocated within the CAMRa domain (60% over land, 12% over sea, 28% on coastlines) from 45 different AMSU overpasses was analyzed to determine the performances of the rain detection tool. Time intervals between the radar observations and the satellite measurements ranged from a few seconds up to 30 min while rain rate (convoluted according to AMSU beam patterns) varies up to 7 mm/h. Over sea, our rain detection tool detects correctly the rain pixels with an HR above 0.7 (NWC breakthrough threshold, Table 1). FAR remains below the NWC breakthrough threshold of 0.4. Over land the rain detection performances exhibit HR below the NWC breakthrough threshold whatever the rain detection tool while the FAR is well below the NWC breakthrough threshold. Study of the HR as a function of the rain rate reveals that over sea (land), HR reaches 0.9 (0.5), 1 (0.5) and 0.7 (0.5) for a rain rate above 1 mm/h suggesting that highly precipitating events can be well detected over sea while over land only 50% of the rainy pixels are detected regardless the rain detection tool. In terms of RR retrieval performance, the rms varies similarly to the one obtained theoretically: the higher the rain rate, the lower the rms with a value around 90% for rain rate ranging from 1 to 6 mm/h.

5. CONCLUSIONS

The potential of mm/submm wave observations for both precipitation detection and quantification has been demonstrated from theoretical calculations. The skills of a frequency set such as planned for the GOMAS mission, with and without the 50 GHz O_2 channels, fully satisfy the user requirements up to the threshold level for NWP and nowcasting applications in terms of rain detection as well as for rain rate retrieval above 1 mm/h. The retrieval of other hydrometeor quantities (e.g., ice, snow, graupel) has also been tested with success, as well as the possibility of estimating the vertical hydrometeor profiles [4, 5].
This opens new perspectives to detect, quantify and track precipitation quasi-continuously on future geostationary missions. The next step requires the validation of instrumental concepts using mm/submm technology on airborne platforms during well-documented measurement campaigns.

ACKNOWLEDGMENTS

This study was supported by ESA under contract 18054/04/NL/FF. Partial support was also provided by EUMETSAT under contract EUM/CO/04/1311/KJG and by CNES under TOSCA contract.

REFERENCES

[1] Chaboureau, J.-P., N. Sohne, J.-P. Pinty, I. Meirold-Mautner, E. Defer, C. Prigent, J. Pardo, M. Mech, and S. Crewell, A midlatitude precipitating cloud database validated with satellite observation, J. Appl. Meteor. Climatol., 47, 1337-1353, 2008.
[2] Meirold-Mautner, I., C. Prigent, E. Defer, J. R. Pardo, J.-P. Chaboureau, J.-P. Pinty, M. Mech, and S. Crewell, Radiative transfer simulations using mesoscale cloud model outputs: Comparisons with passive microwave and infrared satellite observations for midlatitudes, J. Atmos. Sci., 64, 1550-1568, 2007.
[3] Rizzi, R. P. Bauer, S. Crewell, M. Leroy, C. Matzler, W. P. Menzel, B. Ritter, J. E. Russel, and A. Thoss, Cloud, precipitation and large scale land surface imaging (CPL) observational requirements for meteorology, hydrology, and climate, Position paper, version 1.K, Eumetsat, available from http://www.eumetsat.int/Home/Main/What_We_Do/Satellites/Future_Satellites/Post-EPS/index.htm, 2006.
[4] Defer, E., C. Prigent, F. Aires, J. R. Pardo, C. J. Walden, O.-Z. Zanifé, J.-P. Chaboureau and J.-P. Pinty, Development of precipitation retrievals at millimeter and sub-millimeter wavelengths for geostationary satellites, J. Geophys. Res., 113, D08111, doi:10.1029/2007JD008673, 2008.
[5] Mech, M., S. Crewell, I. Meirold-Mautner, C. Prigent, and J.-P. Chaboureau, Information content of millimeter observations for hydrometeor properties in mid-latitudes, IEEE Trans. Geosci. Remote Sens., 45, 2287-2299, 2007.
[6] Kummerow, C., Y. Hong, W. S. Olson, S. Yang, R. F. Adler, J. McCollum, R. Ferraro, G. Petty, D.-B. Shin, and T. T. Wilheit, The evolution of the Goddard Profiling Algorithm (GPROF) for rainfall estimation from passive microwave sensors, J. Appl. Meteorol., 40, 1801 – 1820, 2001.
[7] Pardo, J. R., J. Cernicharo, and E. Serabyn, Atmospheric Transmission at Microwaves (ATM): An Improved Model for mm/submm applications, IEEE Trans. on Antennas and Propagation, 49/12, 1683-1694, 2001.
[8] Pardo, J. R., E. Serabyn, M.C. Wiedner, and J. Cernicharo, 2005: Measured telluric continuum-like opacity beyond 1 THz, J. Quant. Spec. Radiat. Transfer, 96, 537-545, 2005.
[9] Mishchenko, M.I., J. Hovenier, and L. Travis, Light scattering by non-spherical particles. Elsevier, New York, 2000.
[10] Guillou, C., S. J. English, C. Prigent, Passive microwave airborne measurements of the sea surface response at 89 and 157 GHz, J. Geophys. Res., 101, 3775-3788, 1996.
[11] Prigent, C., F. Aires, and W. B. Rossow, Land surface microwave emissivities over the globe for a decade, Bul. Am. Meteorol. Soc., 1573-1584, doi:10.1175/BAMS-87-11-1573, 2006.
[12] Prigent, C., E. Jaumouille, F. Chevallier, and F. Aires, A parameterization of the microwave land surface emissivity between 19 and 100 GHz, anchored to satellite-derived estimates, IEEE T. Geosci. Remote, 46(2), 344-352, 2008.
[13] Evans, K. F., and G. L. Stephens, Microwave radiative transfer through clouds composed of realistically shaped ice crystals. Part I: Single scattering properties, J. Atmos. Sc., 52, 2041-2057, 1995.
[14] Saunders, R., M. Matricardi, P. Brunel, S. English, P. Bauer, U. O'Keefe, P. Francis, and P. Rayer, RTTOV-8 science and validation paper, report NWP-SAF, 44p, 2005.
[15] Bizzarri B et al., GOMAS - Geostationary Observatory for Microwave Atmospheric Sounding, submitted to ESA in response to the call for ideas for the Next Earth Explorer Core Missions, 2005.
[16] Buehler, S. et al., Cloud Ice Water Submillimeter Imaging Radiometer (CIWSIR), Document in response to the ESA Call For Ideas for the Next Earth Explorer Core Missions, 2005.